Magnetic Field Measurements of a Twisted Flux Rope in a Partial Solar Eruption

Presenter:Yuqian Wei
Coauthor:Bin Chen
Sijie Yu
Haimin Wang
Ju Jing
Dale E. Gary

Jul.8th 2021

Abstract

Magnetic flux ropes are the centerpiece of solar eruptions. Direct measurements for the magnetic field of flux ropes are crucial for understanding the triggering and energy release processes, yet they remain heretofore elusive. Here we report microwave imaging spectroscopy observations of an M1.4-class solar flare occurred on 2017 September 6, using data obtained by the Expanded Owens Valley Solar Array. This flare event is associated with a partial eruption of a twisted filament observed in Hα by the Goode Solar Telescope at the Big Bear Solar Observatory. The filament, initially located along the magnetic polarity inversion line prior to the event, undergoes a partial eruption during the course of the flare. This partially erupting filament has a counterpart in microwaves, whose spectral properties indicate gyrosynchrotron radiation from flare-accelerated nonthermal electrons. Using spatially resolved microwave spectral analysis, we derive the magnetic field strength along the filament spine, which ranges from 700--1400 Gauss from its apex to the legs. The results agree well with the non-linear force-free magnetic model extrapolated from the pre-flare photospheric magnetogram. The multi-wavelength signatures of the event are consistent with the standard scenario of eruptive flares, except that the eruption failed to fully develop and escape as a coronal mass ejection. We conclude that the failed fully eruption is likely due to the strong strapping coronal magnetic field above the filament.

Main scientific goal

- Provide measurement of the spatially resolved magnetic field along an active filament in a flare-productive Active Region

Example of:

Magnetic Field Diagnostics through Microwave Spectroscopy imaging Observation

Fleishman et al. 2020

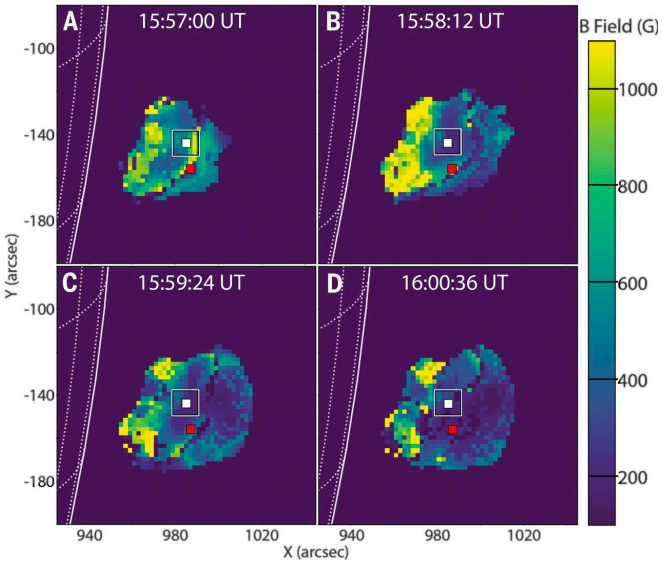

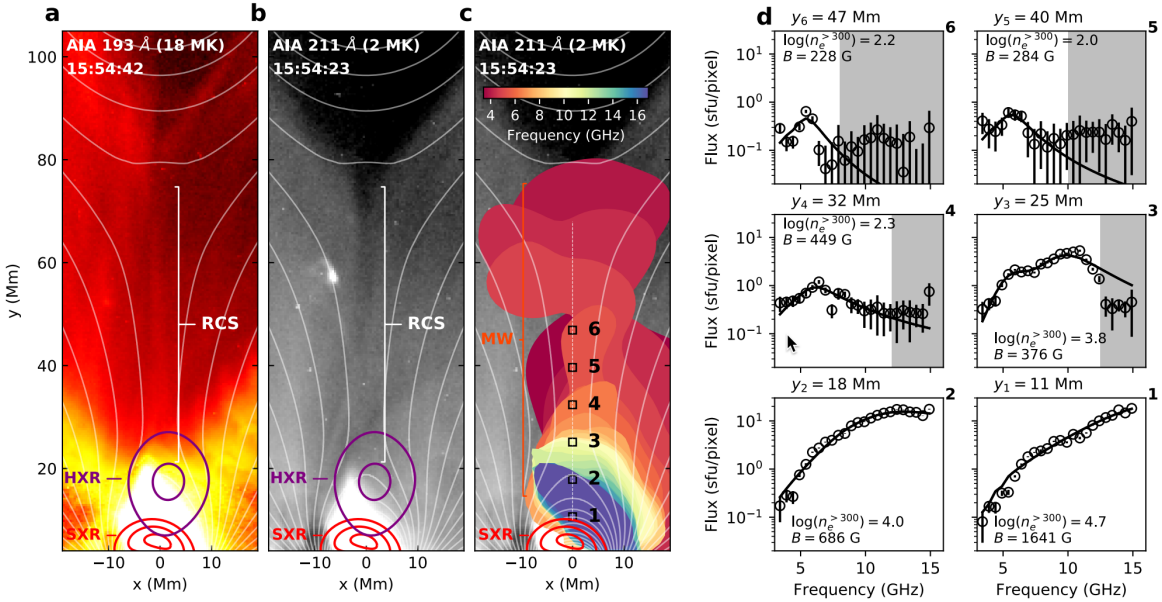

Chen et al. 2020b

Microwave Diagnostics: Gyrosynchrotron

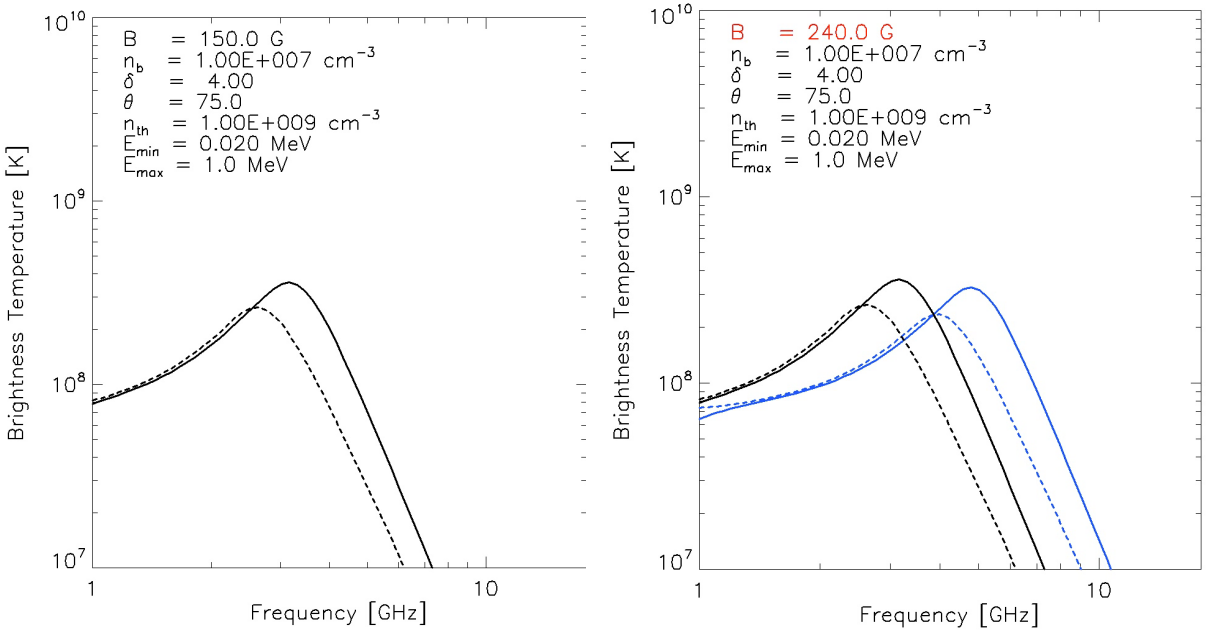

Fleishman et al. 2020

High spectral resolution and comprehensive spectral coverage make EOVSA one of the best observatories in gyrosynchrotron Microwave Diagnostics.

The Expanded Owens Valley Solar Array (EOVSA)

EOVSA

Temporal Res.	1s
Freq Range	1-18GHz
Elements	13
Longest Baseline	~1.0 km

Example of :

Gyrosynchrotron emission in Magnetic Flux Rope(MFR)

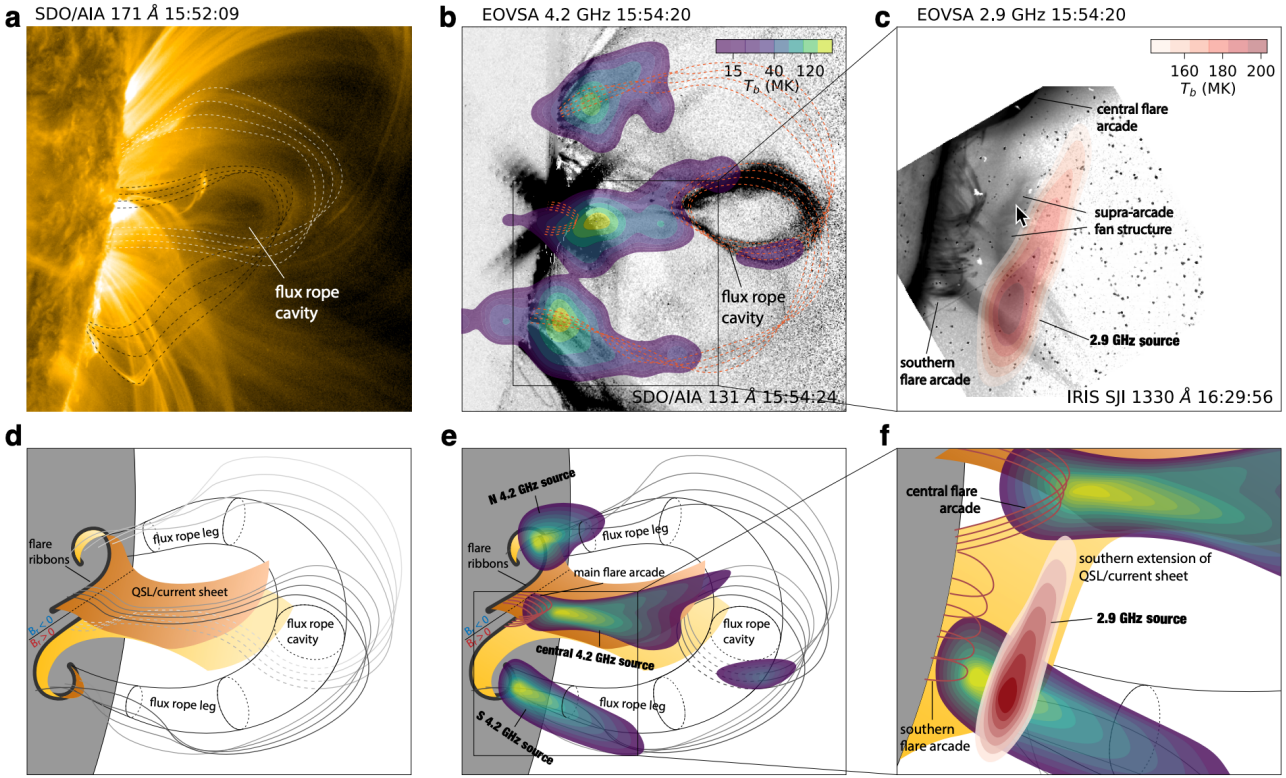

Chen et al. 2020a

Joint Study with BBSO & HMI: B Field of a Filament

BBSO/GST H-α

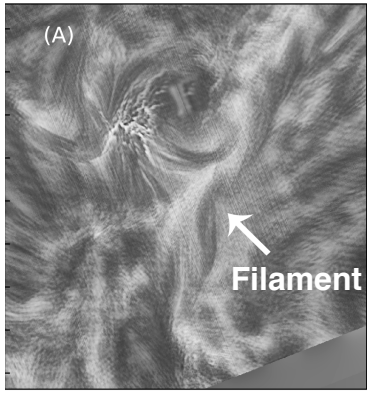

SDO/AIA 1600

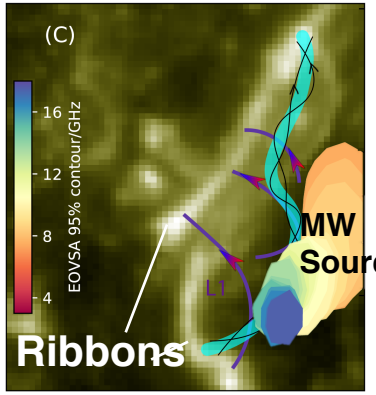

SDO/HMI Magnetogram

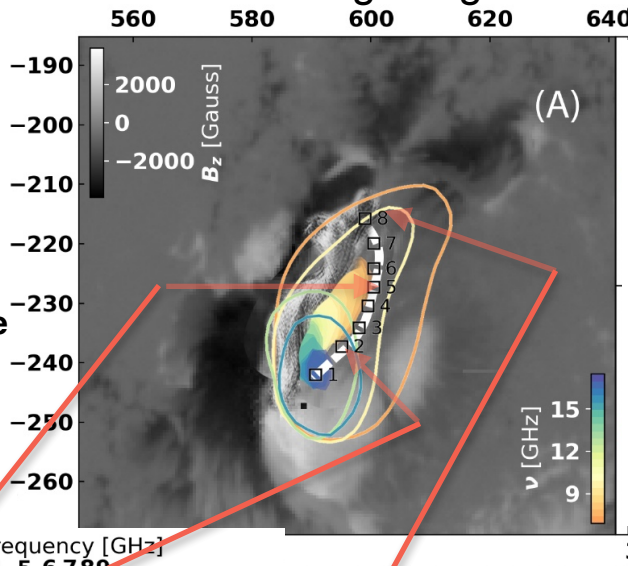

Schematic

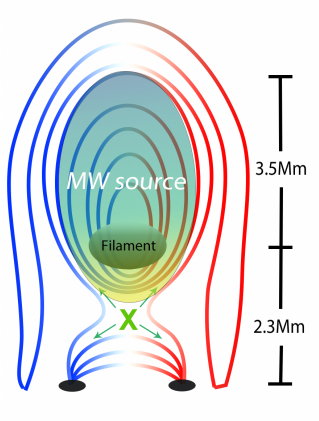

Spatially Resolved Microwave

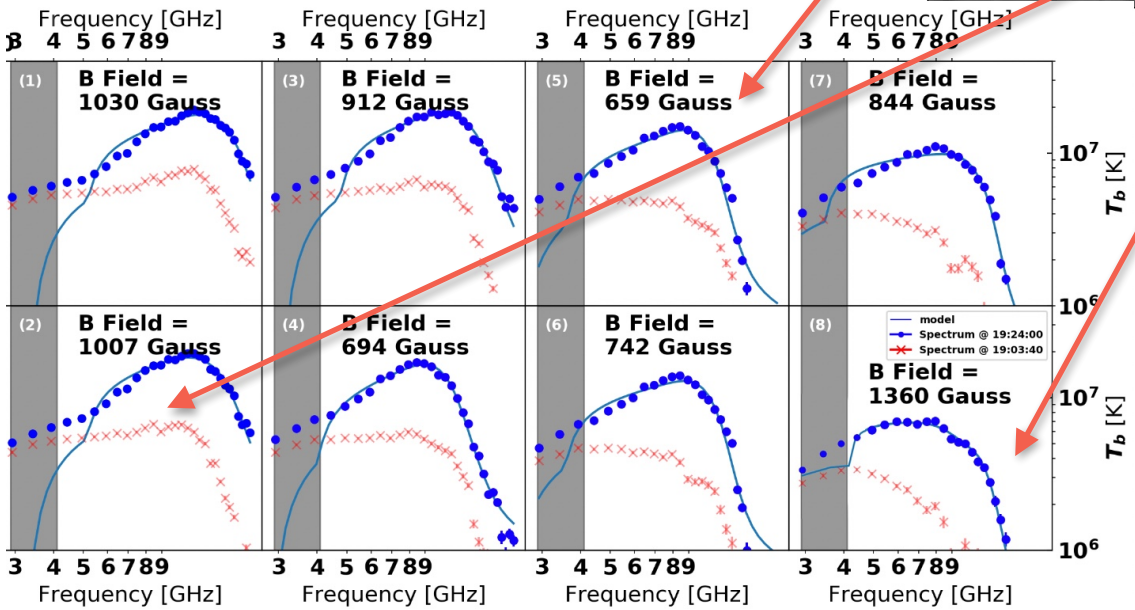

B field at the filament

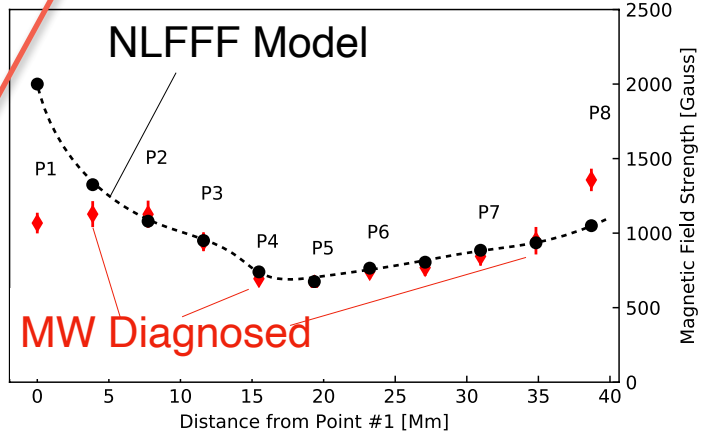

Observation

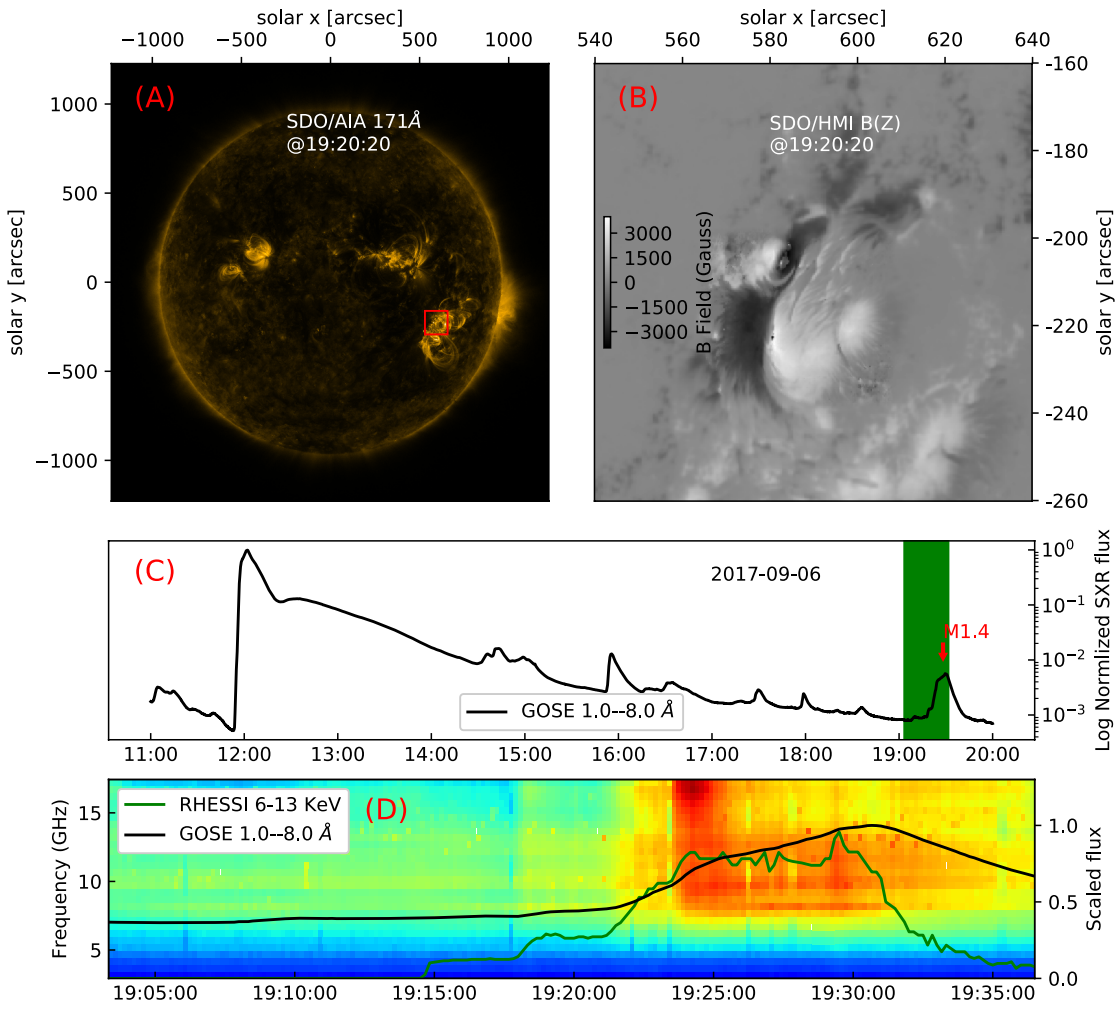

M1.4 Flare
Sep.6th 2017
Peaked:
19:24:00 UT

Data Coverage:
EOVSA
BBSO/GST
RHESSI
…

(A) AR 12673 as observed in EUV by the SDO/AIA 171°A filter band on 2017 September 6 at 19:20:20 UT. (B)Detailed view of the SDO/HMI radial photospheric magnetogram of the core region of the AR (red box in (A)). (C) GOES 1–8A soft X-ray (SXR) light curve from 11 UT to 20 UT on 2017 September 6. The M1.4 flare event under study (marked by the red arrow and the green shaded region) occurs during the late decay phase of the large X9.3 flare (SOL2017-09-10T12:24:00).(D) Background subtracted EOVSA microwave dynamic spectrum from 19:03 UT to 19:37 UT. The black and green curves are for RHESSI 6–13 KeV X-ray and GOES 1–8A light curves, respectively.

Observation

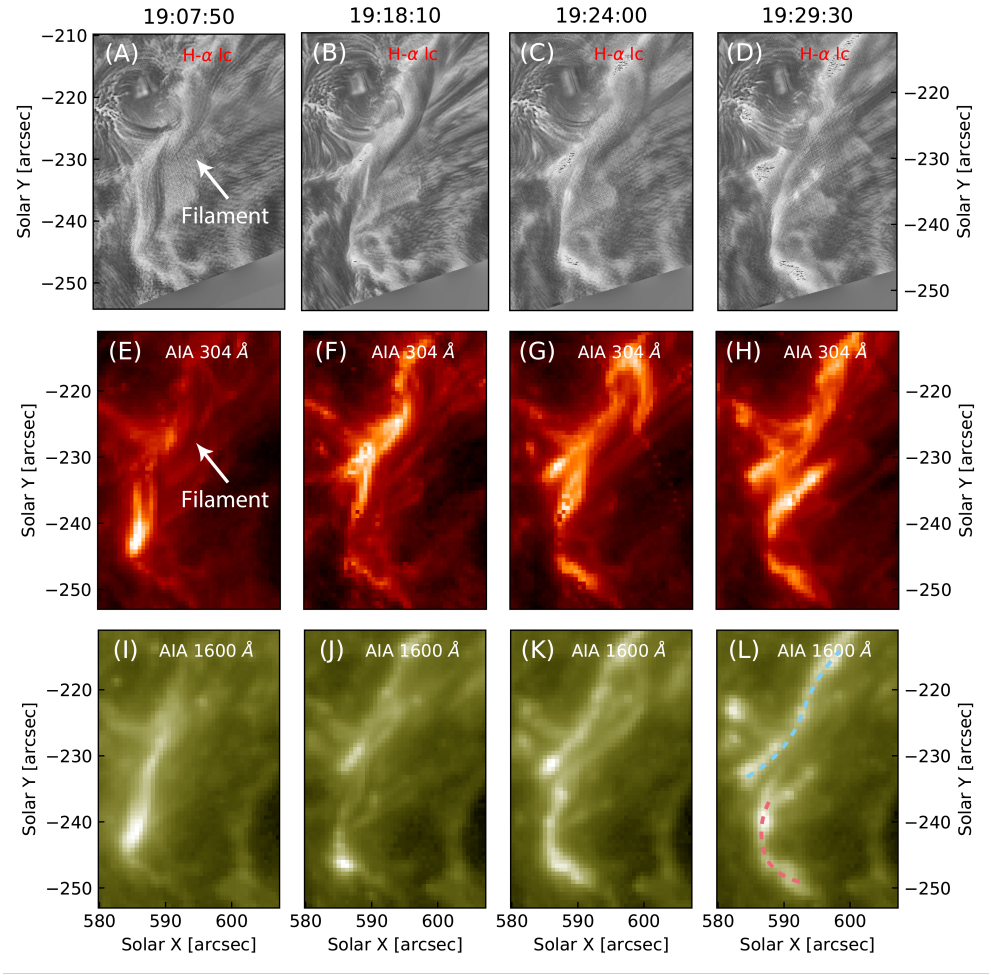

A pre-existing filament

is seen by BBSO/GST in Hα line center image as well as the EUV images before the onset of the event at 19:07:50 UT, 2 ribbons are observed in UV images at footprints of the filament.

Fig2:(A)—(D) BBSO/GST Halpha line center image at four selected times during the event. The filament is marked by the white arrows in the first frame of Hα and SDO/AIA 304Å images. (E)--(H) SDO/AIA 304Å images, in which the dark filament is also seen. (I)--(L) SDO/AIA 1600Å images showing the evolution of the two flare ribbons, which are denoted by the blue and red dashed lines, respectively, in (L)).

Observation

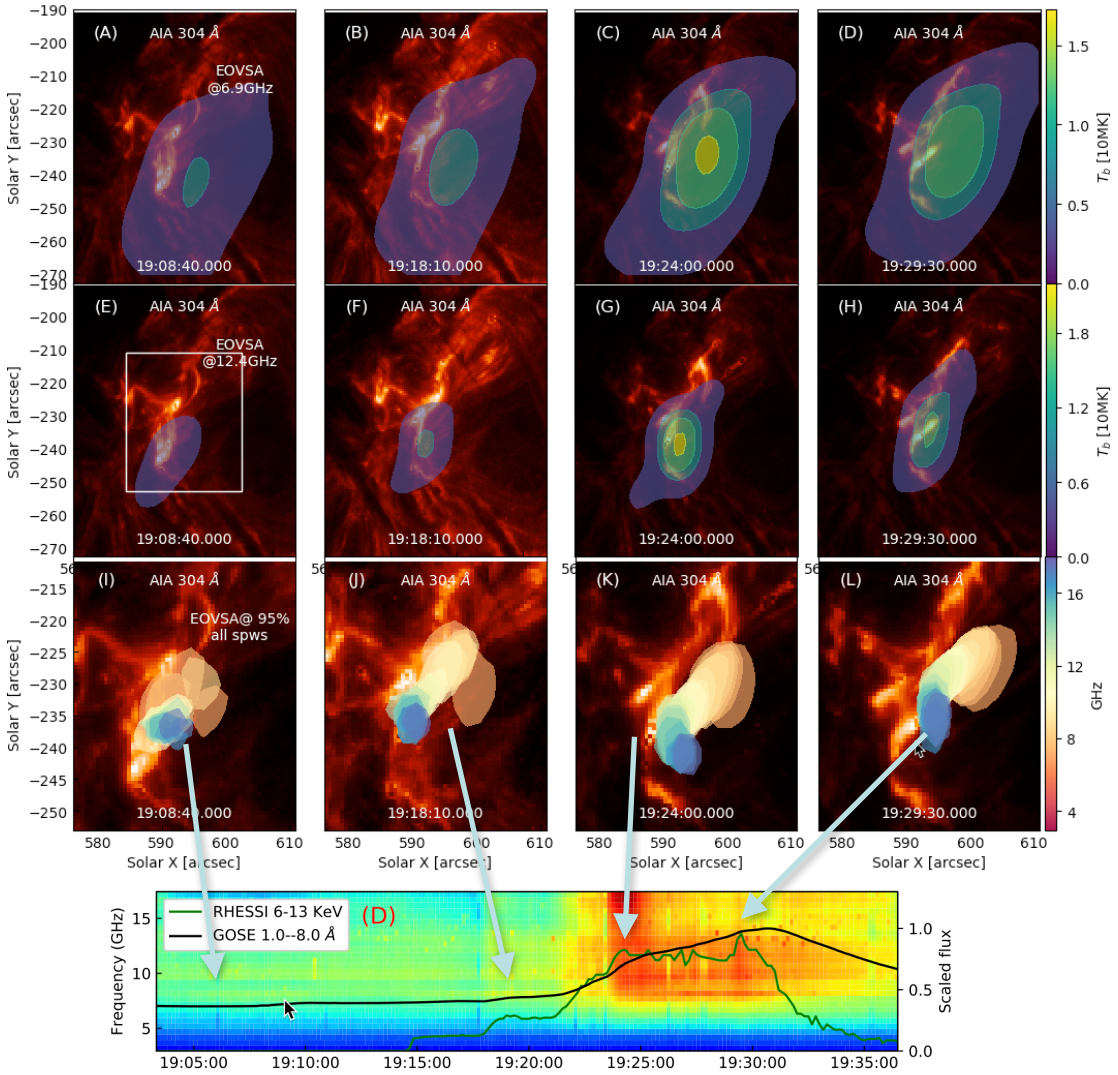

Microwave counterpart of the filament is observed by EOVSA. The microwave source at both frequencies show an elongated shape stretched along the north-west and south-east direction, parallels to the brightened filament seen in the SDO/AIA 304Å images.

Spatial evolution of EOVSA microwave spectroscopic images. (A -- D) Contours of the EOVSA image at 6.9 GHz is over-plotted on SDO/AIA 304A images at selected for times, as same as those in the previous figure. (E -- H) Same as (A -- D), but for the EVOSA 12.4 GHz image. (I -- L) 95% of the maximum brightness at each frequency contours of EOVSA SPW 7 -- 30 (6.4 -- 17.9 GHz) images on SDO/AIA 304A images with a smaller FOV shown as the white rectangle in (E).

Observation

The synchronized motion of:

Microwave source kernel

And

Dark Filament front

indicate that the source comes from the upper part of the flux rope.

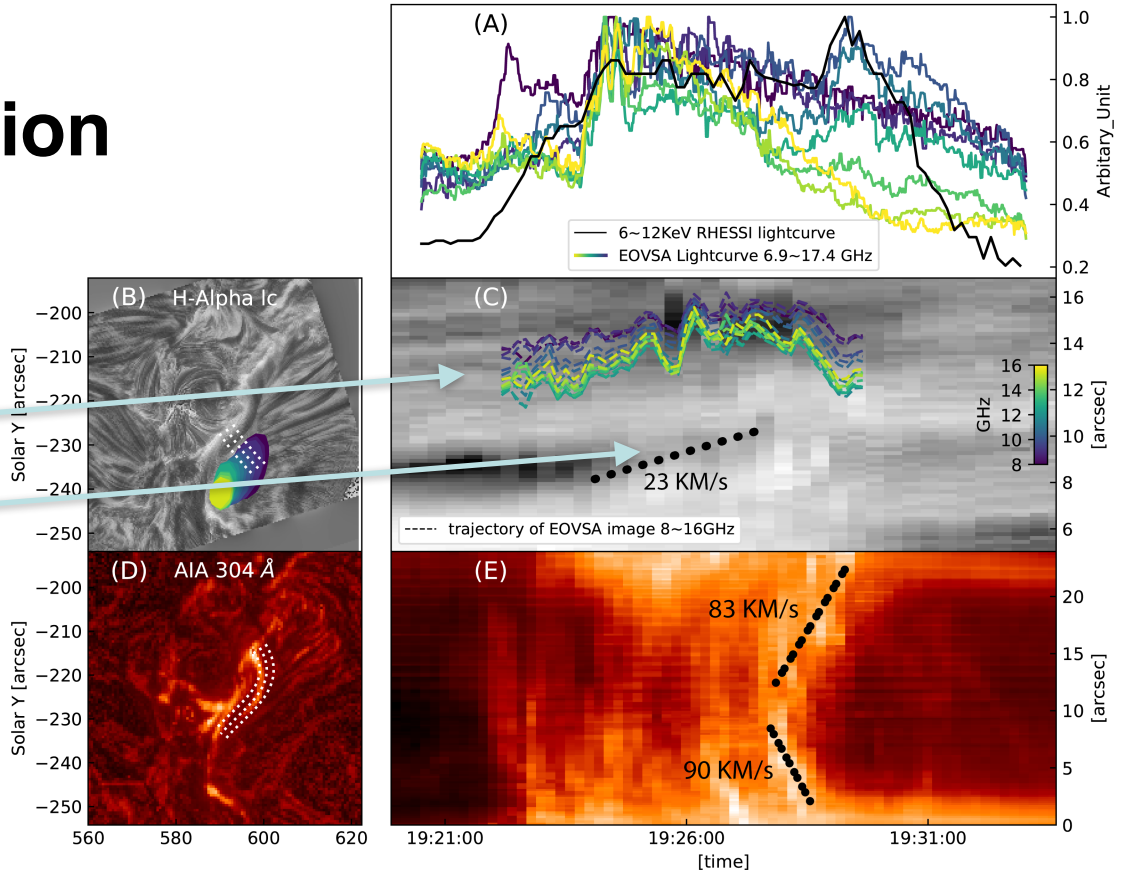

(A) The solid black line indicates the RHSSI X-ray lightcurve at 6 – 13 keV. The EOVSA lightcurves in 7.9 – 17.4 GHz are color-coded by frequencies, as shown in the color bar in (C). (B) 90% contour of EOVSA SPW 10 – 25 (7.9 – 15.9 GHz) image contour and the cut slit (white slit) plotted on BBSO/GST Hαimage at 19:20:20 UT. (C)Time-distance stack plot of BBSO/GST Hαimage from 19:20:00 UT – 19:33:00 UT. The color-coded dashed lines indicate the location of EOVSA images. The dark filament front is pointed by two white arrows. (D) cut slit (white slit) along the filament is plotted on SDO/AIA 304A image at 19:20:20 UT. (E) The time-distance plot along the filament in SDO/AIA 304A image, showing the filament heating and material draining.

Topology Explanation

Observed filament is reproduced in NLFFF extrapolated magnetic field.

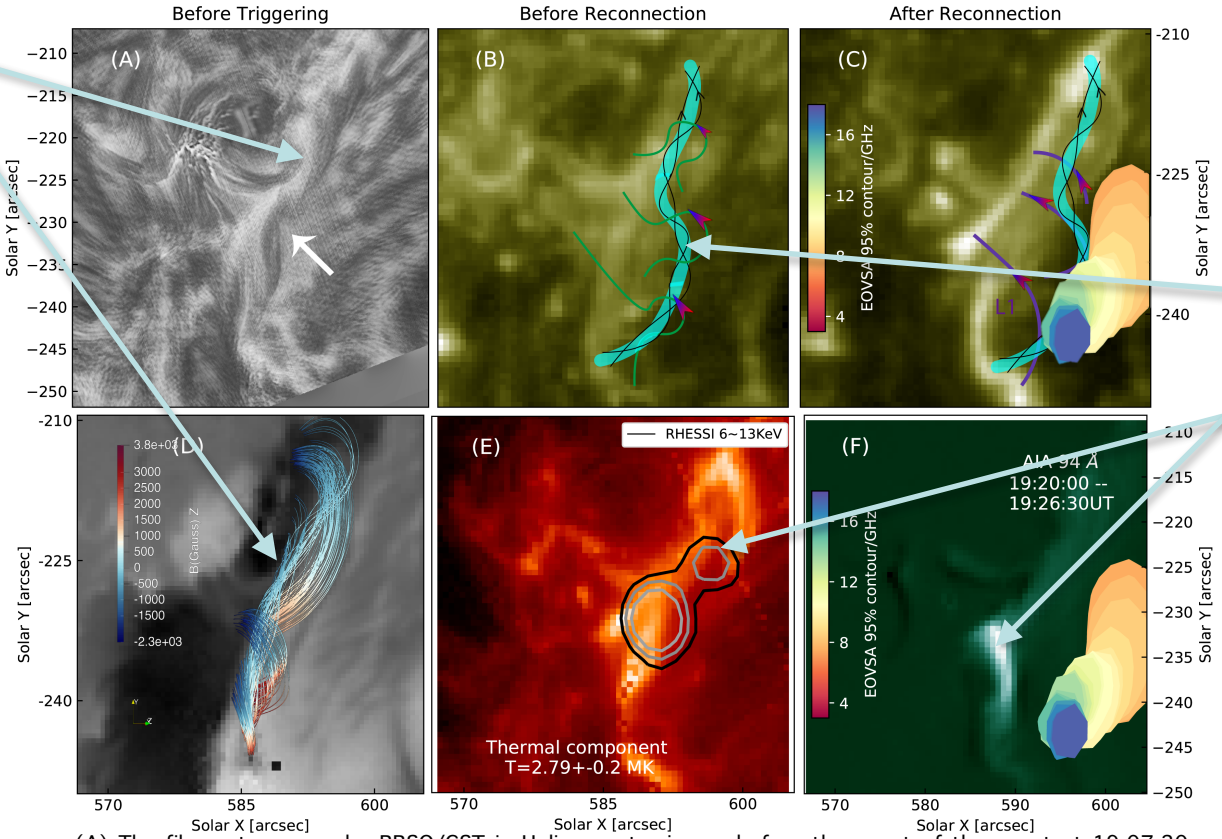

Reconnection Geometry (below the MFR) is revealed by the HXR and EUV observations

(A) The filament as seen by BBSO/GST in Hαline center image before the onset of the event at 19:07:20 UT(denoted by the white arrow). (B) and (C) Schematic of the reconnection induced by the rising filament. The green field linesin (B) and purple field lines in (C) are pre-reconnection and post-reconnection field lines, respectively. The background is thecorresponding SDO/AIA 1600A image showing the two bright ribbons during the post-reconnection phase. EOVSA 6.4–15.9GHz images at 19:26:30 are also shown in (C) as color contours (90% of the maximum). (D) Selected field lines near the PILregion derived from the NLFFF results based on the SDO/HMI vector magnetogram at 19:00 UT. (E) RHESSI 6–13 keV X-raysource (65%, 85%, and 95% of the maximum) overlaid on SDO/AIA 304A EUV image during the impulsive phase. (F) Basedifference SDO/AIA 94A image (19:26:30 - 19:20:00 UT) showing the bright post-reconnection flare arcade. EOVSA 6.4–15.9GHz images (pre-flare-background subtracted in the image domain) at 19:26:30 are also shown.

Result

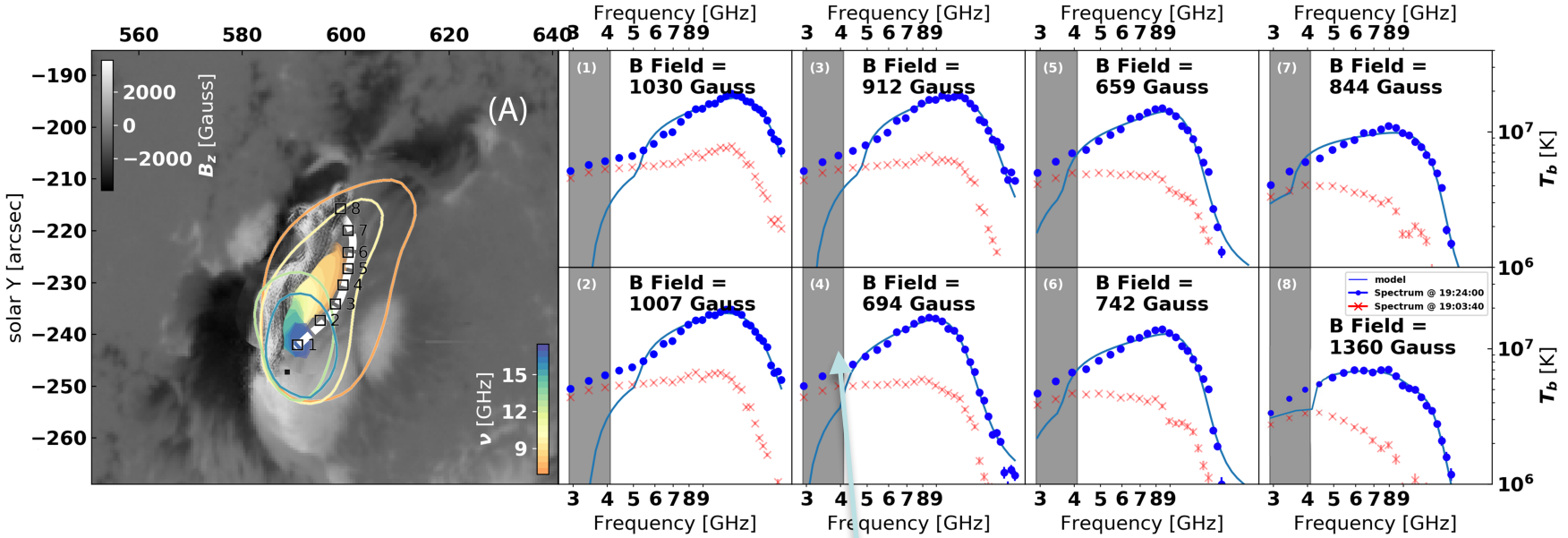

The brightness temperature spectra in 8 points along the flux rope. (A) LOS viewing of the flux rope structure in the NLFFF extrapolated and EOVSA image (pre-flare-background subtracted in the image domain) at selected frequencies in6.9 – 17.9 GHz with 35% and 90% contour level over plotted on a photospheric magnetic field map in the Z component. Points1 – 8 correspond to spectras in (1 – 8). (1 – 8) temporal evolution of the brightness temperature spectra at point 1 – 8 in (A).The spectra at 19:24:00 UT and the best fit model(solid blue circles with error bar and solid blue line). The pre-flare spectra at each points are plotted as the red crosses in (1 – 8).

12 points were selected along the microwave counterpart of the MFR(8 out of 12 are plotted). The corresponding background subtracted spectrum is fitted to the isotropic gyrosynchrotron to obtain the **magnetic field strength** (and other 3 free parameters, number density of thermal and non-thermal electrons, energy index of non-thermal electrons) at each point.

Result

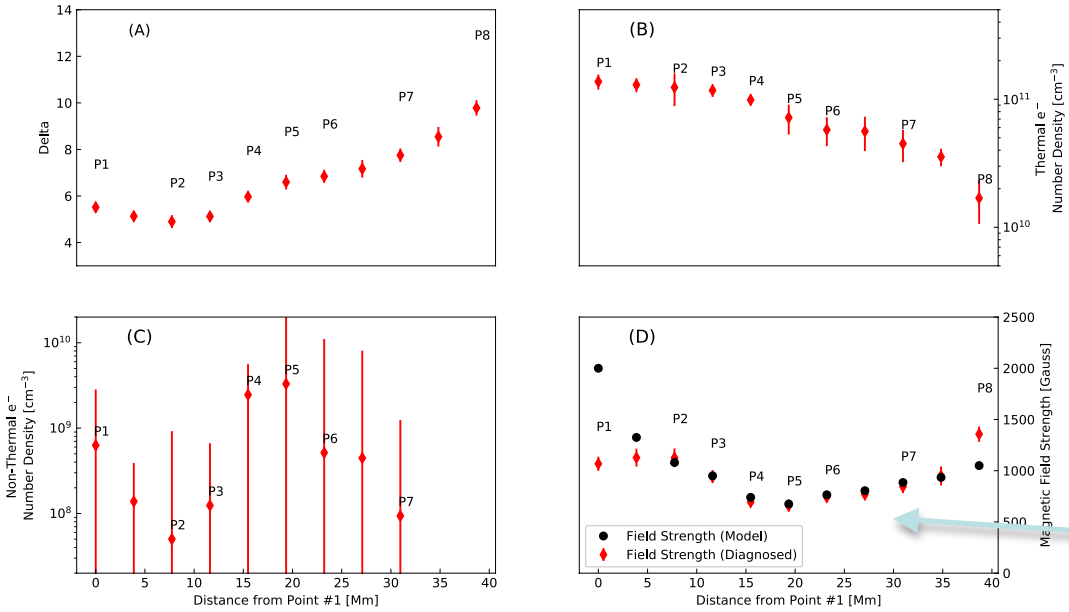

Critical free parameters' distribution along with a selected magnetic field line in the extrapolated vector coronal magnetic field. The error is constrained by Markov chain Monte Carlo (MCMC) sampling methods.
(A -- D) Spatial distribution of power-law index, thermal electron density, non-thermal electron density, and magnetic field strength, respectively. (D) the magnetic field strength of the extrapolated field line are plotted as black dots.

Microwave diagnostics reveals a reasonable distribution of the four parameters along microwave counterpart of the MFR. The accelerated electrons are concentrated at the southern foot point. The magnetic field strength increases with distance from the footpoints.

Comparison:

A field line in the NLFFF extrapolated magnetic field, which goes through the 12 points, is selected to be compared with the microwave diagnostics. The results are qualitatively consistent.

Partial Eruption

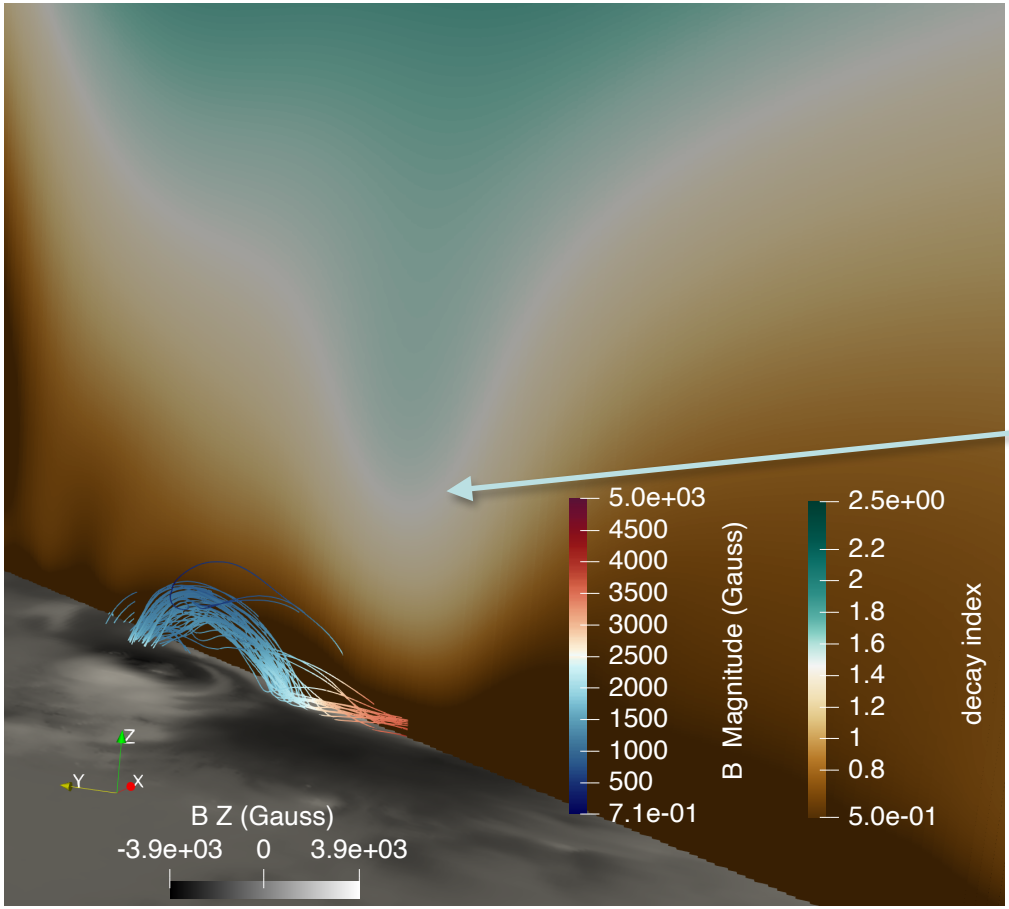

Decay index distribution above the flux rope. The decay index is calculated from the potential extrapolated magnetic field while the flux rope is from the NLFFF extrapolation.

The MFR locates where the Decay index $n = -\frac{d \ln B_{ex}}{d \ln R}$ is lower than a typical value for eruption, **1.5**

Constrain from the overlying magnetic field may make the eruption fail.

Summary

- we provide the first measurement of the spatially resolved magnetic field along an active filament in a flare-productive AR. The microwave-constrained results are qualitatively consistent with those derived from the NLFFF extrapolation.

Topology Explanation

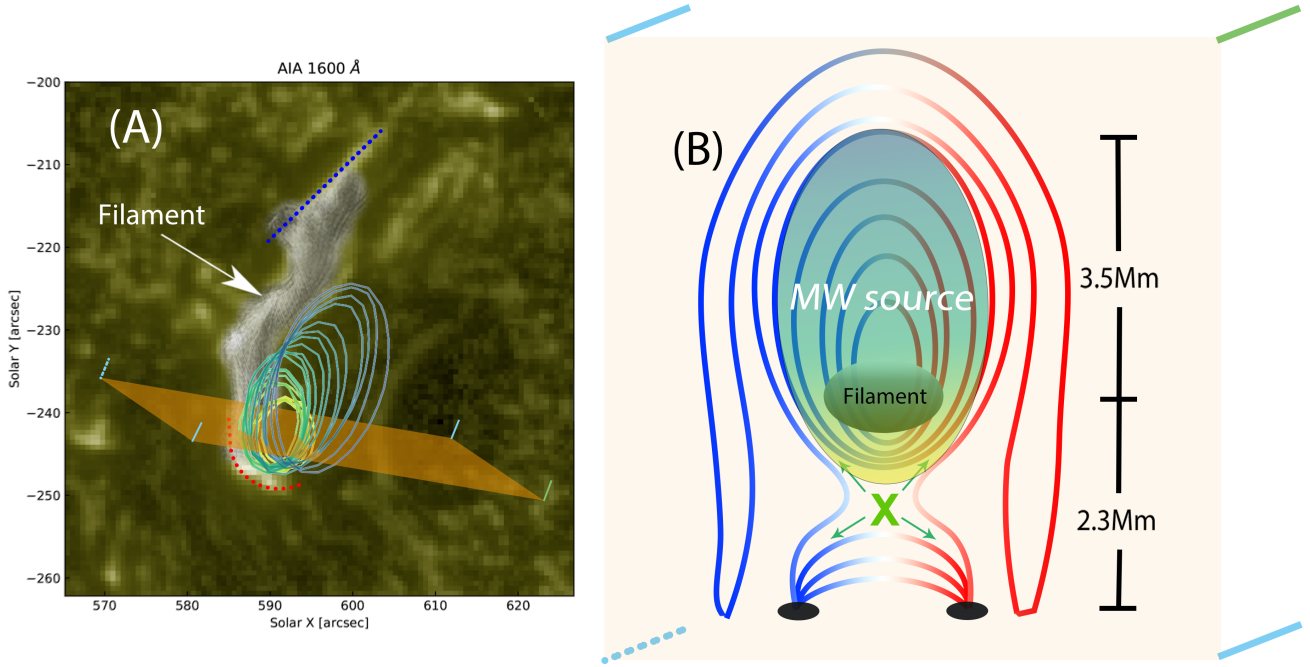

Schematic cartoon that shows the relation between the filament and the microwave source. (A) 80% contours of EOVSA images SPW (6.9 -- 15.9 GHz) image contour are plotted over the filament from Halpha image. (B) Schematic cartoon of the cross-section of the flux rope, is made out of the orange surface in (A).

The cool, dense filament is chromospheric-temperature material supported near the concave-upward bottoms of the MFR field lines. Meanwhile, accelerated electrons due to magnetic reconnection induced by the partial eruption of the MFR can enter the extended MFR cavity following the newly reconnected field lines, producing the multi-frequency nonthermal microwave emission above the filament.

The associated CME

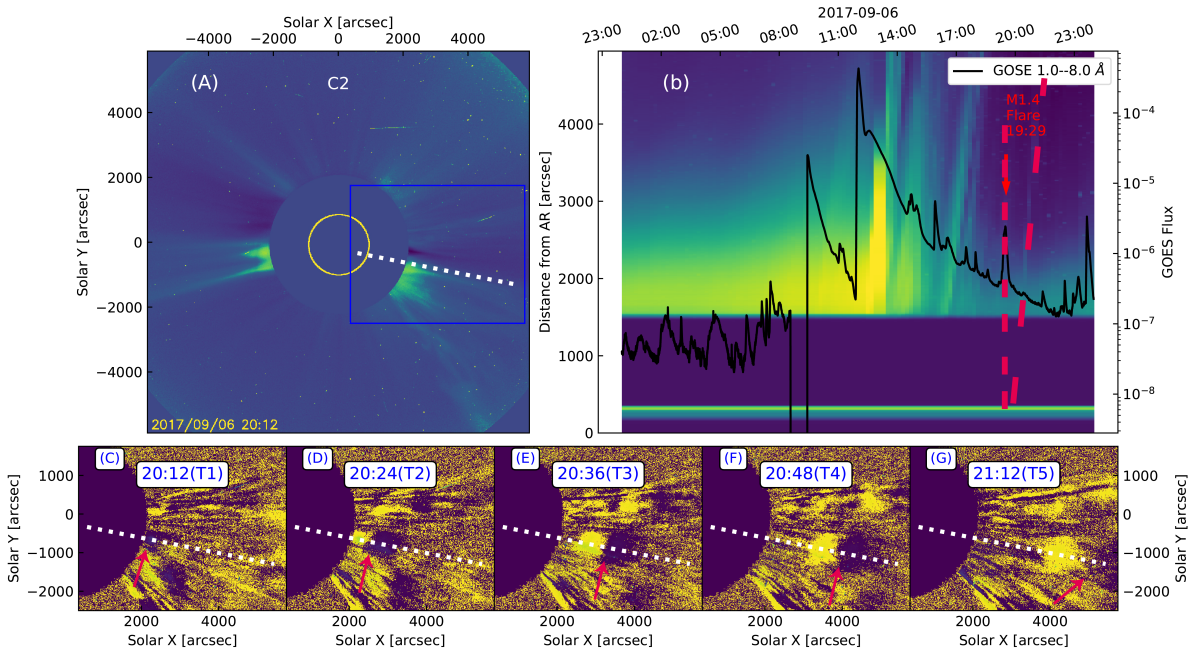

(A) LASCO C2 image at 20:12 UT. The chosen slit starts from the lower corona at AR 12673, points out toward the edge of LASCO C2 image, shown as the white dashed line. (B) Time-distance plot of LASCO C2 image at 2017-09-06 from the slit in (A). GOES lightcurve of the day is overplotted. The vertical red dashed line indicates the time when the event occurs. The tilted dashed line goes through the associated CME and traces back to the lower corona. (C -- G) Running differential image of LASCO C2 at selected time. The filed-of-view is shown as the blue box in (A). The CME feature is pointed with red arrows.